Electrochemical Performance of Porous Ni-Cu Anodes for Direct Methanol Fuel Cells

R. Abdel-Karim [1,*], Y. Reda[2], K. M. Zohdy[3], A. Abdelfatah[1], S. El-Raghy[1]

[1] Corr. and Surface Treatment Lab., Dept. of Metallurgy
Faculty of Engineering- Cairo University, Giza 12613, Egypt.
[2] Chemical Engineering Department, Higher Institute of Engineering and Technology, New Damietta 34517, Egypt.
[3] Higher Technological Institute, 10th of Ramadan city, Egypt
*E-mail: randaabdelkarim@gmail.com

Transition metal 3D porous foams based on Ni and Cu were prepared using Hydrogen Bubble Dynamic Template "DHBT" technique, from an acidic solution containing Ni-Cu salts as a source for Ni-Cu deposits. The morphology of the deposited films was affected by the current density and deposition time. At low current density and short deposition time (30 sec), smooth films composed of angular grains, with few randomly distributed isolated dendrites were detected. At high current density, typical ramified dendritic morphology was developed. The Ni content of the deposited layer varied from 68.49- 87.86 %. The electrocatalytic behavior of these layers was evaluated using potentiodynamic, cyclic voltammetry and electrochemical impedance test in acidic 1 M methanol solution. From potentiodynamic test results, increasing the deposition current density as well as deposition time lead to more anodic and current density, reflecting high electro catalytic behavior towards methanol oxidation. In addition, the forward peak intensity and total charge measured by cyclic voltammetry increased under the effect of higher applied current density and longer deposition time having a positive effect on the electrochemical activity of the Ni-Cu NPMFs deposited. According to EIS data, the charge transfer resistance (R_p) decreased as the current density as well as electrodeposition time increased. The lowest polarization resistance (51.7Ω) required for high electrocatalytic behavior was detected for porous Ni-Cu layers electrodeposited at 2 Amp/cm^2 and deposition time 150 sec.

Keywords: Fuel cells; Ni-Cu deposits; Dynamic Hydrogen template; SEM; Ramified Dendrites; Potentiodynamic test ; Cyclic voltammetry; EIS.

1. INTRODUCTION

Direct Methanol fuel cells "DMFC" are a good power source for supporting a wide range of portable and low power applications [1]. They DMFC has the advantage of not requiring a fuel reformer,

which allows simple and compact design. As a fuel, methanol has some advantages over hydrogen; it is liquid at room temperature and pressure, it is stable in contact with acidic membranes, has limited toxicity, high energy density and low theoretical electro-oxidation potential (E°) comparable to that of hydrogen. In addition, it is cheaper to manufacture and easier to handle and transport [2]. Pure methanol has an energy density 15 times higher than the energy density of a Li-ion battery and one order of size larger than H_2 stored in a pressurized tank (at 200 bar) or in a metal hydride system (4–5%). But, the energy density of methanol is lower than that of conventional liquid fuels such as gasoline and diesel [3].

Direct methanol fuel cells have some limitations. Crossover of Methanol from the anode to the cathode through the polymeric electrolyte membrane, low activity of some methanol electro-oxidation catalysts, and the high cost of components inhibit the large-scale applications of DMFC [3]. The performance of DMFC technology and higher efficiency would be achieved by solving the methanol crossover problem [5-7]. The last decade has brought significant progress in the fundamental DMFC research, especially in the anode and cathode electrocatalysis using membrane–electrode structure optimization, cell design and nanoporous metallic foams (NMFs) [8].

The advantages of nanoporous metallic foams "NMFs" include remarkable electrical conductivity, large surface area, high pore volume, and accessibility of active species to the internal surfaces for chemical, catalytic, as well as electrocatalytic reactions. The NMFs with specific architectures may dramatically accelerates mass and charge transfer relevant to chemical and energy transformation processes [9-10]. Several research has been made to improve the electro-oxidation of methanol by modifying the nanostructured metallic foams (NMFs) [11-12]. For examples, **a** rolling technique was applied for the development of porous carbon electrodes for direct methanol fuel cells containing platinum and platinum-ruthenium catalysts [13]. A macroporous 3D architectures of self-assembled MWCNT surface decorated with Pt nanoparticles anodes for DMFC were prepared using an ice segregation induced self-assembly (ISISA) process [14]. Ion implantation method was applied for the production of high stability Ag nanoparticles (NPs) on a flexible 3D nickel foam (NF) electrode coated Nafion membranes (N-AgNPs/NF) [15].

The dynamic hydrogen bubble template (DHBT) technique has been applied for the production of 3D nanostructured metallic foams. This technique has several advantages over conventional ways such as low-cost and simplicity. Exchange current densities for the metals commonly electrodeposited, from fast to slow kinetics are (log i^0/A cm^2) Pt (-3.1), Pd (3.0), Ni (-5.21), Cu (-5.37), Au (-5.4), Ag (-7.85). Metals such as Pt and Pd will thus generate higher volumes of H_2 at a specific overpotential [16].

A potential prospect of the non-Pt based porous materials as an electrochemical catalyst has been revealed, though their activity is still lower than that of Pt-base catalysts [17-18]. Arunachalam [19] demonstrated the synthesis of mesoporous nickel-cobalt oxide (Ni-Co-O) anodes using the microwave synthesis method. Wang [20] applied the anodization approach for obtaining highly porous Ni O anodes. Yuan [21] studied the catalytic behavior of nanoporous nickel-copper-phosphorus amorphous alloy (NPNiCuP) and nanoporous nickel-copper crystalline alloy (NP-NiCu).

Electrodeposition of porous Ni-Cu arrays on different substrates has been thoroughly studied [22-26]. The aim of this work is the production of porous Ni-Cu deposits using Hydrogen Bubble Dynamic Template (DHBT) technique in acidic bath containing Ni-Cu salts as a source for Ni-Cu alloy.

Different ranges of current densities from 1-2 A/cm^2 with different ranges of time from 30-150 sec will be involved. The effect of applied current density as well as deposition time on the morphology and composition of the metallic foams are to be investigated using SEM and EDAX analysis. The corrosion and electrocatalytic behavior of the obtained Ni-Cu deposits towards methanol oxidation will be studied using potentiodynamic, cyclic voltammetry, and electrochemical impedance test in acidic methanol solution. This work focus on optimizing the electrodeposition parameters to produce nano-structured foams with properly tailored morphology to enhance mass and charge transfer processes. The preparation of optimally combined bimetallic Ni-Cu electrodes will lead to the formation of anodes of improved catalytic properties and stability required for direct methanol fuel cells.

The lowest polarization resistance, R_p (51.7 Ω), required for high electrocatalytic behavior was detected for porous Ni-Cu layers electrodeposited at 2 Amp/cm^2 and deposition time 150 sec. In this case, the deposited layer composed of 70.66% Ni, 19.98%Cu and 1.36% O.

2. EXPERIMENTAL TECHNIQUES

2.1 Testing Materials and Surface Pretreatment.

The substrate used for the electrodeposition process was 301 stainless steel, delivered in the form of polished sheets (0.4 mm thick) with the chemical analysis presented in Table 1.

Table 1. Chemical analysis of stainless steel substrate.

Element	C	N	Si	V	Cr	Mn	Co	Ni	Fe
wt.%	0.0471	0.11	0.643	0.142	18.6	1.32	0.173	7.32	Rem.

The specimens were machined to be of 4 cm long and 1.5 cm width. Before electrodeposition, all samples were subjected to the electrolytic activation pretreatment in a solution of 37% HCl (wt. percent) at room temperature for 2 min. This was followed by rinsing distilled water to remove any traces of chemicals.

2.2 Electrodeposition.

The electrodeposition cell was composed of rod-shaped graphite anode and a rectangular stainless steel cathode, connected to the positive and negative poles of dc power supply type Chroma 62000P-100-25 with a Chroma 62000P software.

The two electrodes were immersed in an electrolyte containing Ni and Cu salts in addition to some additives. Based on the work of Zhang [27], all the bath parameters such as chemical composition, pH, temperature, deposition current density, and deposition time are illustrated in table 2.

Table 2. Electrolytic bath composition and electrodeposition working conditions for synthesizing porous Ni-Cu electrodeposited alloys [27].

Parameter	Value
$NiSO_4.6H_2O$	0.5 M
$CuSO_4.5H_2O$	0.01 M
H_2SO_4	1 M
HCl	0.05 M
H_3BO_3	0.1 M
Sodium citrate tribasic dehydrate	0.2 M
Working parameters	
Time (sec)	30, 90, 150
Current density (A/cm^2)	1, 1.5, 1.8, 2
pH	2

2.3 Electrochemical Tests

All electrochemical measurements were carried out using Gamry PCI300/4 Potentiostat/ Galvanostat/ Zra analyzer, connected to a personal computer. A three-electrode side wall cell containing Ni-Cu NPMFs supported on stainless steel substrate with an active area of 0.87 cm^2 as a working electrode, Pt counter electrode, and SCE reference electrode. Polarization tests were carried out at a scan rate of 2 mV/min at 25 °C. The Echem Analyst 5.21 statistically fits the experimental results to the Stern-Geary model for a corroding system. The routine automatically selects the data that lies within the Tafel's region to the corrosion potential from OCP. The Echem Analyst calculates the corrosion potential, corrosion current density, anodic and cathodic slopes.

In EIS technique a small amplitude ac signal of 10mV and frequency spectrum from 100 kHz to 0.01 Hz was impressed at the open circuit potential (OCP) and impedance data were analyzed using Nyquist plots. The charge transfer resistance, Rp was calculated from the diameter of the semicircle in Nyquist plot.

Cyclic voltammetry tests were conducted by sweeping linearly the potential from the starting potential into the positive direction at a certain scan rate till a required potential value and then reversed with the same scan rate till the starting potential to form one complete cycle. This process was repeated at different scan rates. All measurements were carried out using 1M C_2H_5OH + 0.5M H_2SO_4 electrolyte at room temperature.

3. RESULTS AND DISCUSSION

3.1 Surface Morphology and Chemical Analysis
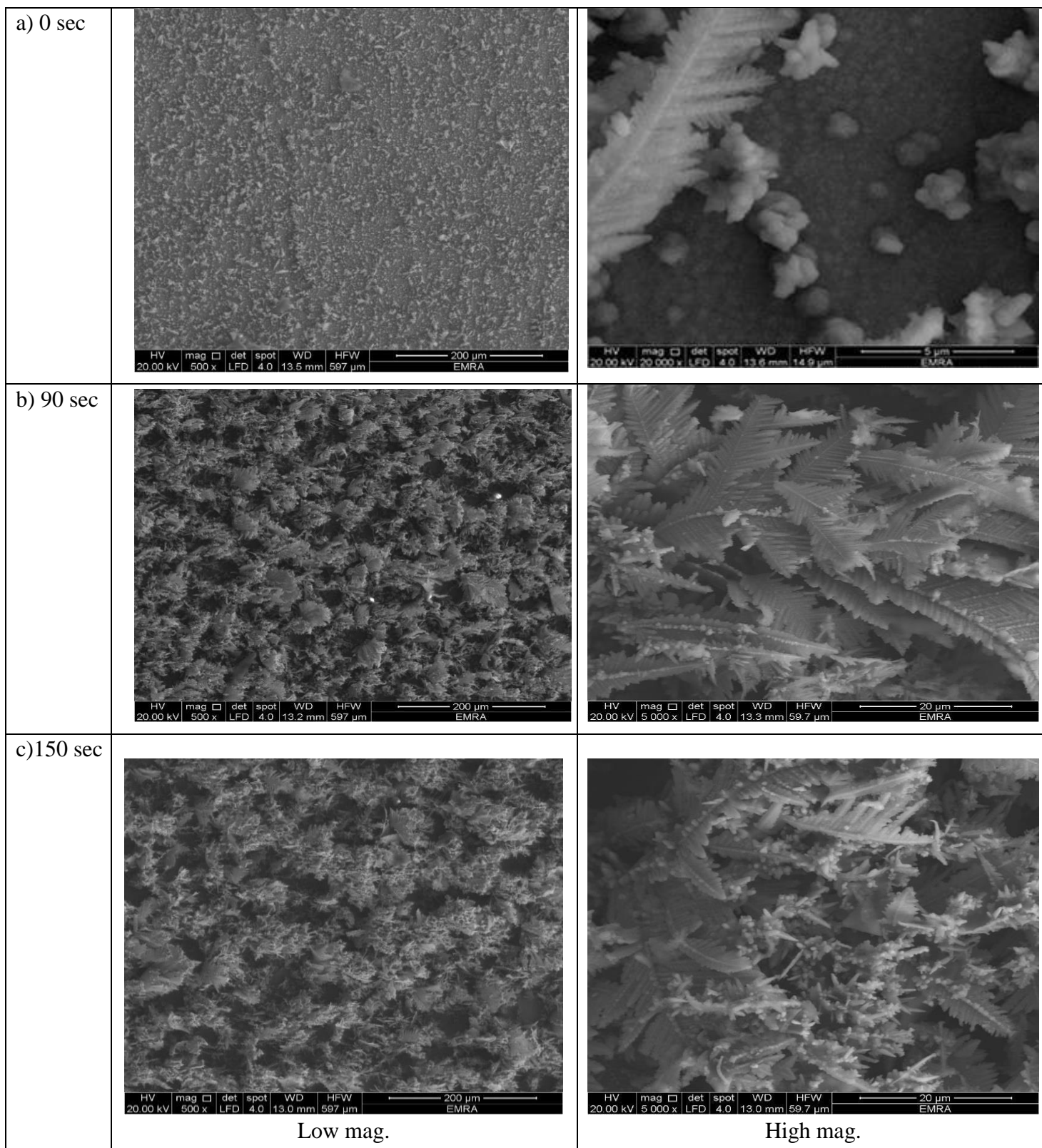
Figure 1. SEM images of porous Ni_{18}–Cu layers electrodeposited on AISI 304 Stainless steel for 30, 90, 150 sec. at current density 1 A/cm^2.
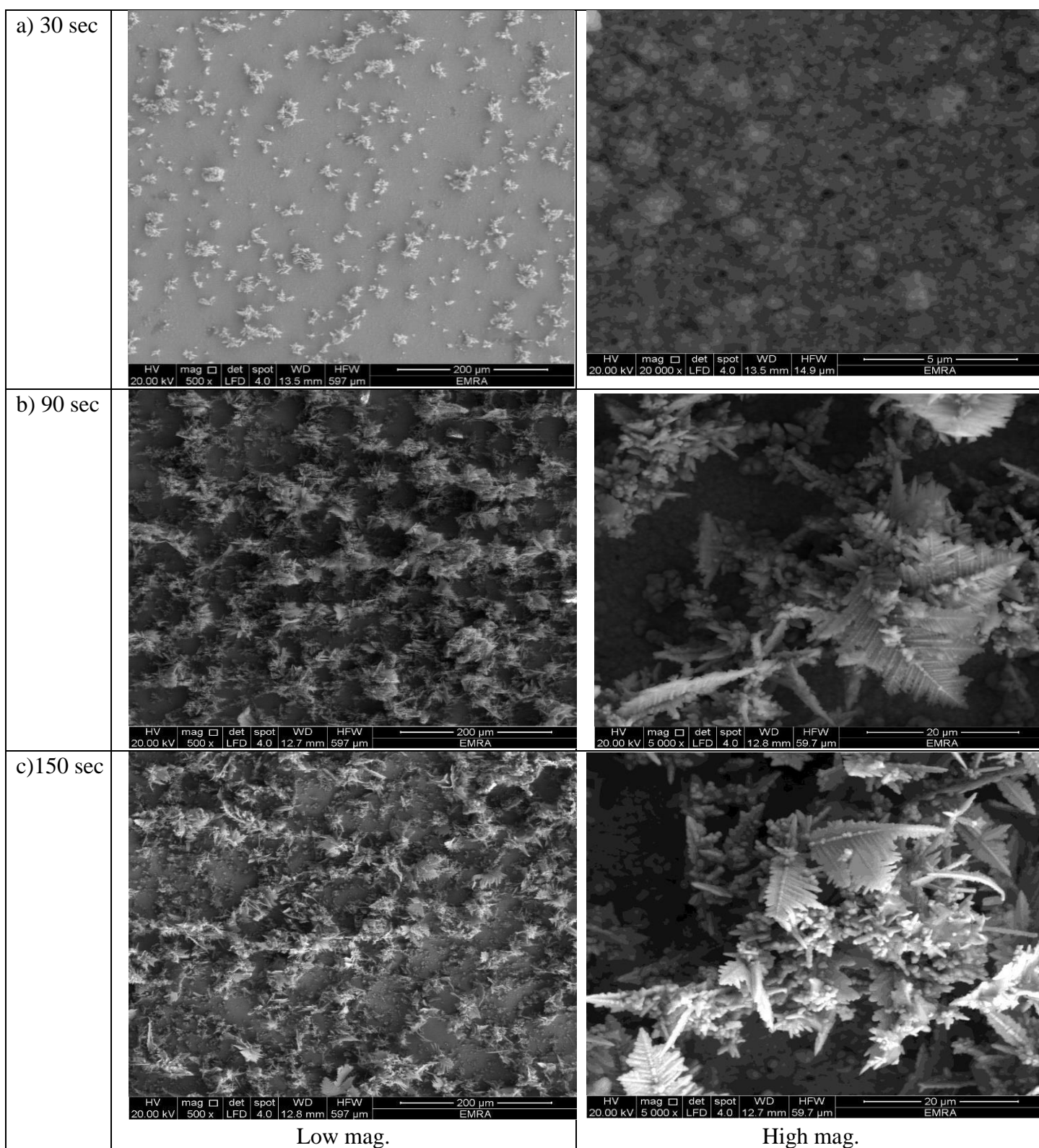
Figure 2. SEM micrographs of porous Ni–Cu layers electrodeposited on AISI 304 Stainless steel for 30, 90, 150 sec. at current density 1.5 mA/cm^2.
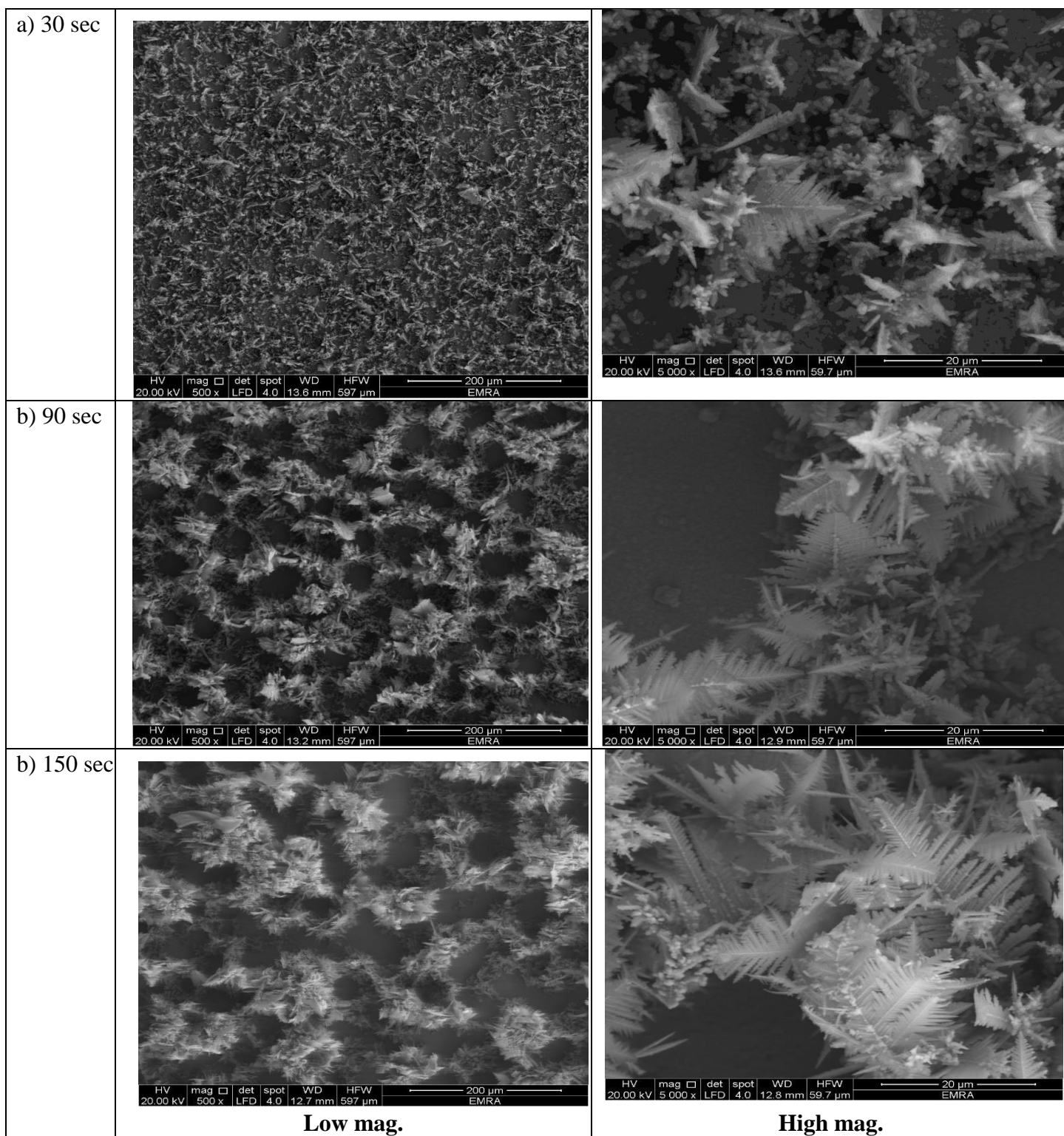
Figure 3. SEM micrograph of porous Ni–Cu layers electrodeposited on AISI 304 stainless steel for 30, 90, 150 sec. at current density 1.8 mA/cm^2.
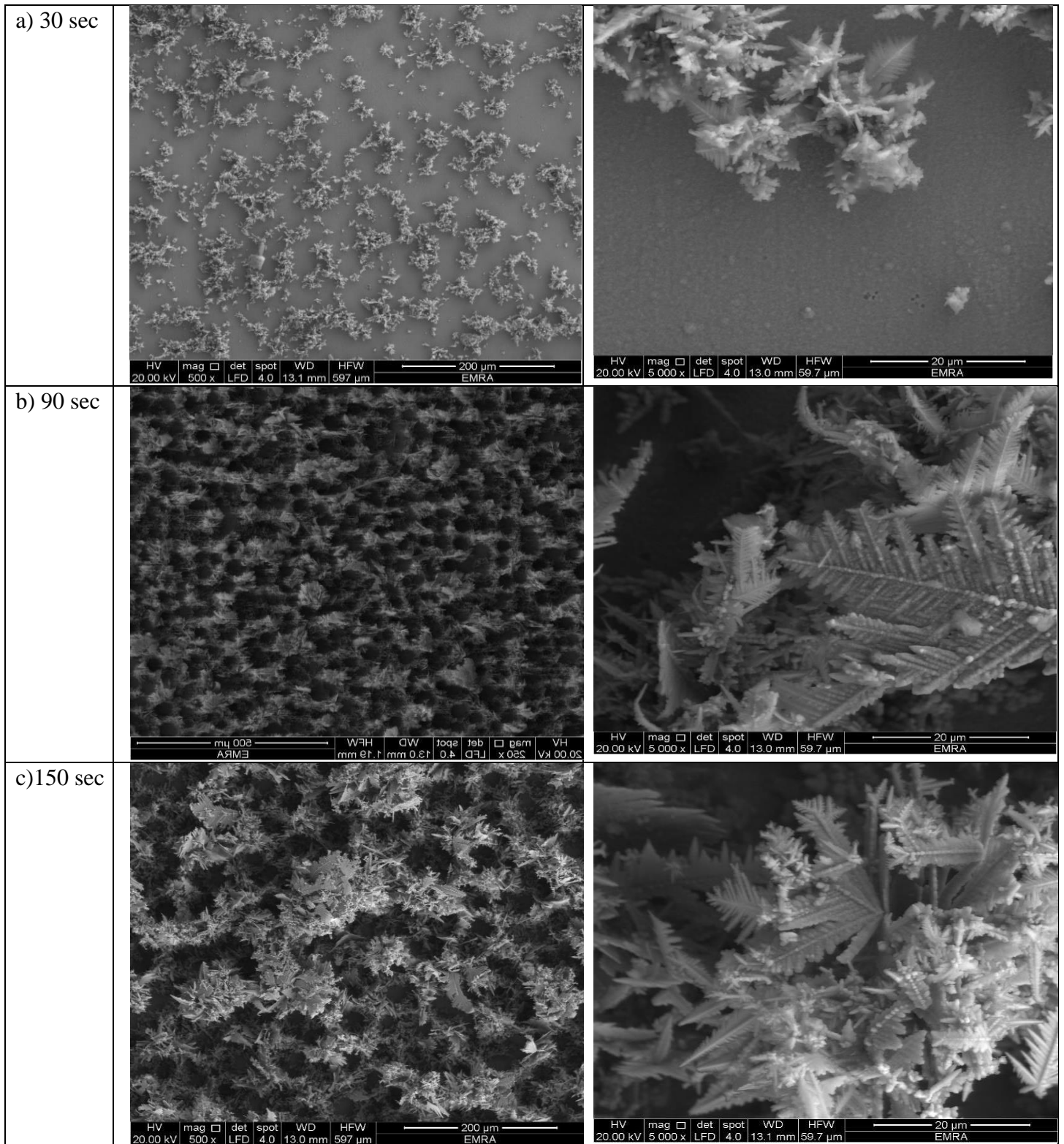
Figure 4. SEM micrographs of porous Ni–Cu layers electrodeposited on AISI 304 Stainless steel 2 A/cm^2 for 30, 90, 150 sec.

Figures 1-4 illustrate the morphology of porous Ni-Cu electrodeposited alloys produced by electrodeposition using a high cathodic current. The formation of pores result from the intensive hydrogen (H$_2$) bubble evolution during the electrodeposition process. The porous structure results from

the so-called "Hydrogen Bubble Templating Mechanism". The templating mechanism of hydrogen bubbles for controlling the pore structure evolution in the electrodeposited copper foams was firstly proposed by Zhang [28].

The resulting Ni-Cu films present a foam-like morphology with randomly distributed nearly circular pores, with open dendritic structure walls. Increasing the current density will lead to formation of fine more ramified dendrites. For short deposition time (30 sec), only smooth films composed of angular grains, with randomly distributed isolated dendrites, are formed.

Euge´nio [29], explained the dendritic growth of electrodeposited porous metal as follows; Firstly, at the early stages of deposition, a continuous layer at the foam/ substrate interface will be formed, providing a complete coverage of the substrate. Consequently, the hydrogen bubbles will form at the dense layer and not on the substrate material itself. Due to the intensive hydrogen evolution, the hydrodynamic conditions near the electrode surface will be changed. At this stage, the thickness of diffusion layer is reduced, hindering the diffusion control necessary for dendritic growth, leading to the formation of continuous and dense layer will be formed. Secondly, with further increase in deposition time and due to the high cathodic current density applied, the agitation provided by hydrogen evolution is no longer sufficient to supply sufficient metal ions to be deposited at the substrate. Finally, the deposition process becomes diffusion controlled leading to the formation of porous dendritic structure [29-30].

From figures (1-4), as the deposition time was further increased (90 and 120 sec), 3D Ni-Cu layers with randomly distributed pores were detected. The 3D structure of the foams was favored with increasing the deposition time, due to the increase of the foam thickness and mass. In addition, as the deposition time increases (Figure 4), the dendrites assumed a fern-like structure with secondary and tertiary branching leading to the formation of a non-compacted pore wall. It can be concluded that, the porosity of the metallic foams arises not only from the existence of pores but also from the formation of pore walls with open dendritic structure. The continuous thin layer formed at the substrate during the early stages of electrodeposition is still visible for all samples.

According to Nikolic [31] there are different types of holes/craters in the deposits. One type presents a nearly circular shape and originates from the formation of hydrogen bubbles at the substrate around which the metal will deposit. A second type of craters presents an irregular shape and their formation may be explained by the nucleation and growth of adjacent metal grains that will join the closely formed agglomerates and thus form irregular holes.

3.2 EDX Chemical Analysis

Table 3 shows the EDX analysis of porous Ni-Cu electrodeposited alloys. The main elements detected were nickel and copper with variable contents. Some residual amounts of oxygen were detected. Depending on the applied current density and deposition time, the Ni content ranges from 68.49% up to 87.86%. The corresponding copper content is in the range 10.80% - 26.72%. In general, increasing both the deposition time and applied current density leads to an increase of the Ni content in the porous Ni-Cu electrodeposited alloys.

Table 3. EDX analysis of porous Ni-Cu electrodeposited alloys.

Element	Electrodeposition time, sec		
	30	90	150
1 mA/cm2	Chemical Analysis, %		
Ni	68.49	73.52	84.26
Cu	24.57	23.74	12.83
O	6.96	2.74	2.91
1.5 mA/cm^2			
Ni	85.70	82.06	82.39
Cu	9.95	16.08	13.32
O	4.36	1.86	4.29
1.8 mA/cm^2			
Ni	80.42	72.42	73.76
Cu	15.80	26.72	25.66
O	3.78	0.86	0.57
2 mA/cm^2			
Ni	84.14	87.86	70.66
Cu	12.45	10.80	19.98
O	3.41	1.34	1.36

3.3 Potentiodynamic Polarization Test
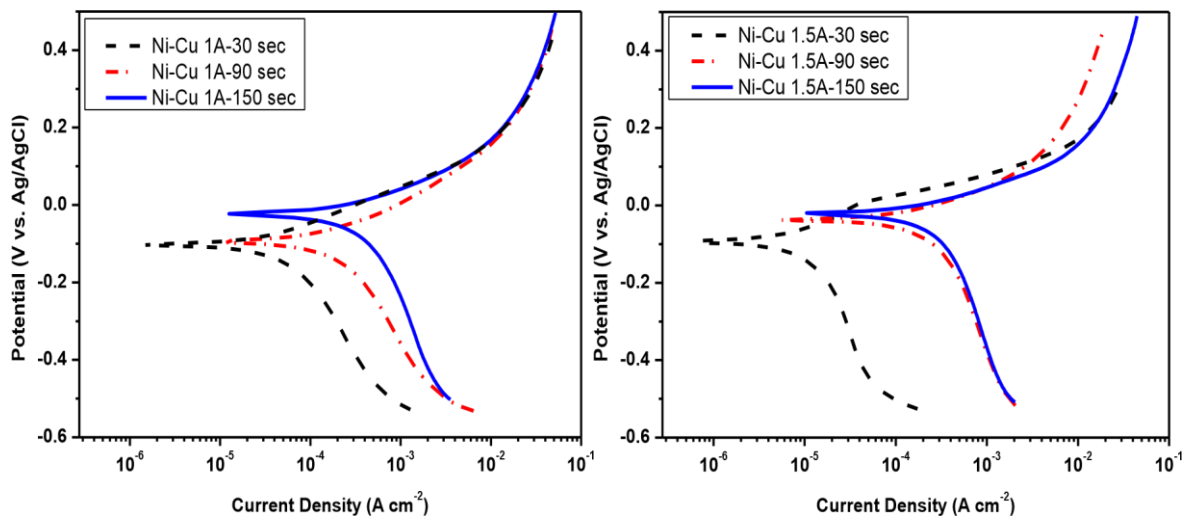
a) 1 A/cm^2 b) 1.5 Am /cm^2
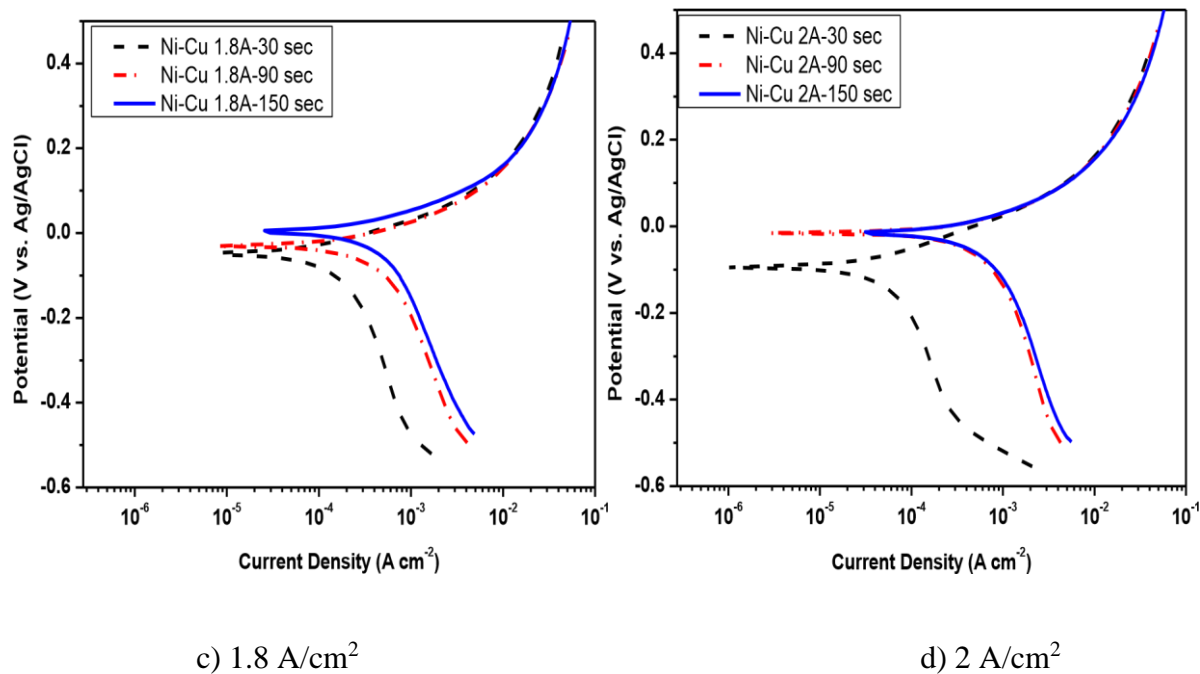
c) 1.8 A/cm^2 d) 2 A/cm^2

Figure 5. Polarization curves for porous Ni-Cu electrodeposited alloys in 1M methanol acidic solution at 25°C

The potentiaodynamic polarization curves of porous Ni-Cu electrodeposited alloys tested in 1 M Methanol+ 0.5M H_2SO_4, as a function of current density as well electrodeposition time are illustrated in figure 5. The corresponding corrosion data such as; corrosion potential, corrosion current, corrosion rate as well as anodic and cathodic Tafel's constants are summarized in table 4. The corrosion rate was in the range of 4.4-426.8 mpy. Meanwhile, the corrosion potential values were in the range of -170 to – 3.6 mv.

The corrosion rate also increased by increasing current density as well as deposition time. The lowest corrosion rate (4.4 mpy) was registered for porous Ni-Cu layers that were electrodeposited at a current density 1.5A for 30 sec. In this condition, smooth deposites composed of angular grains, with some randomly distributed isolated dendrites, are formed (Fig. 2-a). Meanwhile, the highest corrosion rate (426.8 mpy) was detected for porous Ni-Cu layers that were electrodeposited using a current density 2 amp/cm^2 for 150 sec. According to EDX analysis, these layers were containing 70.66% Ni, 19.98%Cu and 1.36% O. Referring to the SEM, the surface morphology was characterized by the formation of fine dense ramified dendritic structure (Fig. 4-c).

From Table 4 the values of the Tafel's slopes βa range from 92 to 288 mV dec^{-1}. The higher corrosion current as well as corrosion rate values for Ni-Cu deposits, compared with that of the steel substrate (11 μm/y) [32], are due only to the oxidation of methanol and not due to any corrosion of the nanocrystalline Ni-based alloy surface. The highest current density was registered for Ni-Cu alloys deposited at current density 2 A/cm^2 for 150 min (Figure 5-d).

Table 4. Polarization data for the corrosion of Ni-Cu NPMFs electrodeposited alloys at different current density 1-2 A/cm^2 and different times 30, 90,150 sec using 1M methanol acidic solution at 25°.

Electrode	$E_{corr.}$ mV	$I_{corr.}$ µA/cm ^{2}	Tafel's slopes		Corrosion rate (C.R.) mpy
			β_a mV/decade	β_c mV/decade	
Ni-Cu 1A/cm^2-30 s	-102.0	49.1	116	340	25.4
Ni-Cu 1A/cm^2-90 s	-170.0	249.0	288	364	129.0
Ni-Cu 1A/cm^2-150 s	-23.6	294.0	288	364	152.4
Ni-Cu 1.5A/cm^2-30 s	-93.0	8.4	110	364	4.4
Ni-Cu 1.5A/cm^2-90 s	-36.6	214.0	120	388	110.9
Ni-Cu 1.5A/cm^2-150 s	-21.2	303.0	120	651	156.9
Ni-Cu 1.8A/cm^2-30 s	-48.2	141.0	92	442	73.1
Ni-Cu 1.8A/cm^2-90 s	-29.5	516.0	138	564	267.1
Ni-Cu 1.8A/cm^2-150 s	-3.6	570.0	138	599	294.9
Ni-Cu 2A/cm^2-30 s	-93.8	48.9	92	396	25.3
Ni-Cu 2A/cm^2-90 s	-15.1	727.0	149	652	376.2
Ni-Cu 2A/cm^2-150 s	-15.0	824.0	149	653	426.8

3.4 Cyclic Voltammetry
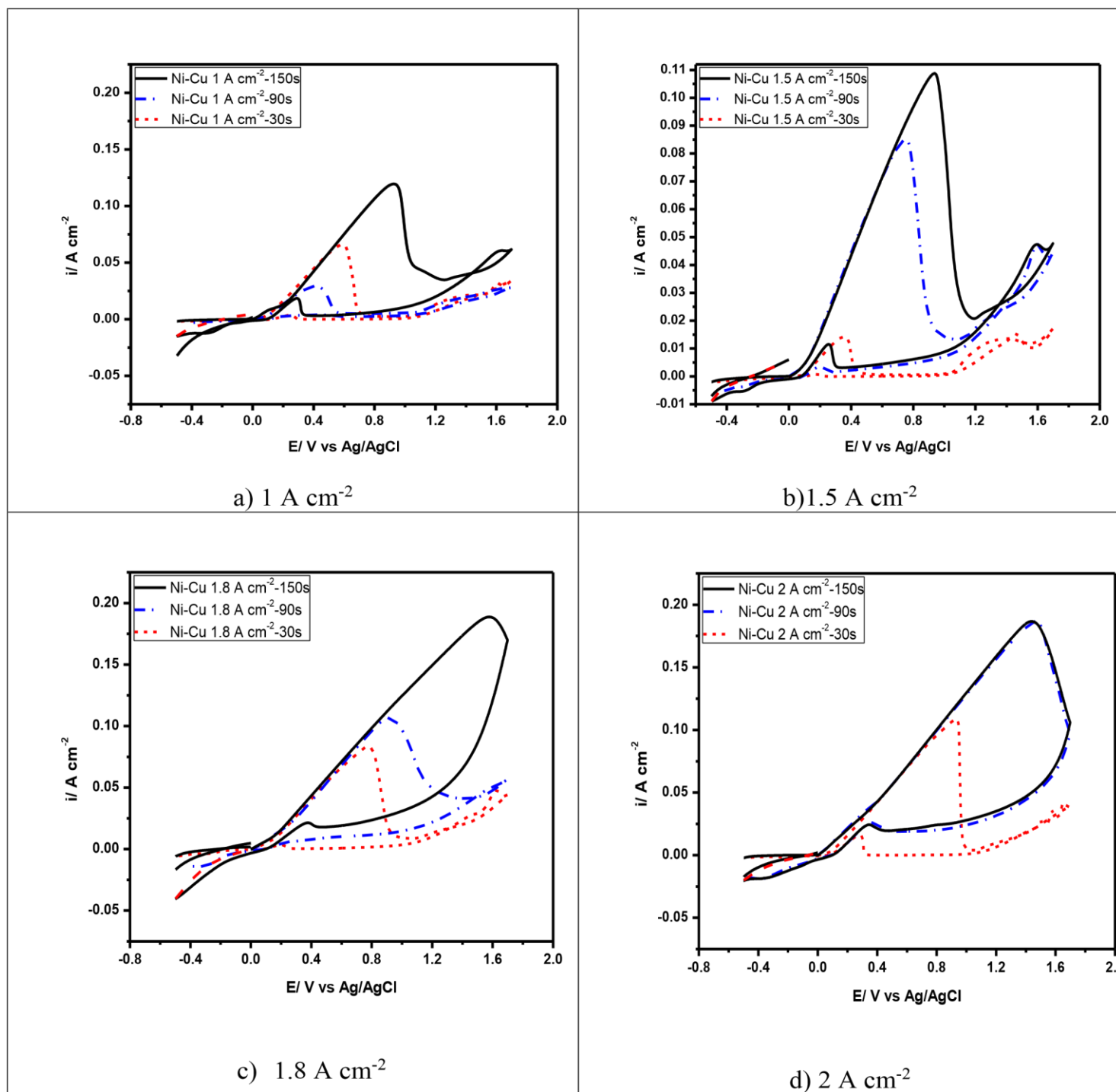
Figure 6. Cyclic voltammograms of porous Ni-Cu electrodeposited alloys tested in 1M methanol acidic
solution.

The electrochemical behavior of porous Ni-Cu electrodeposited alloys was evaluated in 1 M
acidic methanol solution by cyclic voltammetry. The obtained voltagrams are presented in figures 6 and
7, for current densities 1-2 A/cm². It is worse to mention that, the forward peak intensity and total charge
measured by cyclic voltammetry increased under the effect of higher applied current density and longer
deposition time having a positive effect on the electrochemical activity of the Ni-Cu NPMfs deposited

The voltammograms of porous Ni-Cu electrodeposited alloys show a two redox peaks in the potential range of -0.4 to +1.6 V. The forword peak is due to the oxidation of methanol, while the backword peak is related to the corresponding cathodic reaction. Methanol electro-oxidation is complex reactions occurring in a series of parallel reaction pathways [32-35]. Methanol has a low theoretical oxidation potential (0.02 V) comparable to that of hydrogen (0.0 V). Thus, it can be an efficient fuel at low temperatures.

The reaction mechanism for acidic DMFC is:

Anode reaction:

$$CH_3OH + H_2O = 6H^+ + CO_2 + 6e- \quad (1)$$

Cathode reaction:

$$1.5\ O_2 + 6H^+ + 6e- = 3H_2O \quad\quad (2)$$

Overall reaction:

$$CH_3OH + 1.5\ O_2 = 2H_2O + CO_2 \quad\quad (3)$$
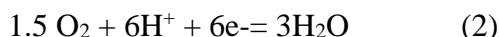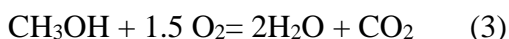
Therefore, every molecule of methanol provides 6 electrons that pass from the anode to the cathode via external circuit providing electric current [35-36].

a) at 150 sec with different deposition current 1-2 A cm^{-2} (scan rate 100 mV s^{-1})

b) 2 A cm^{-2} with different scan rates
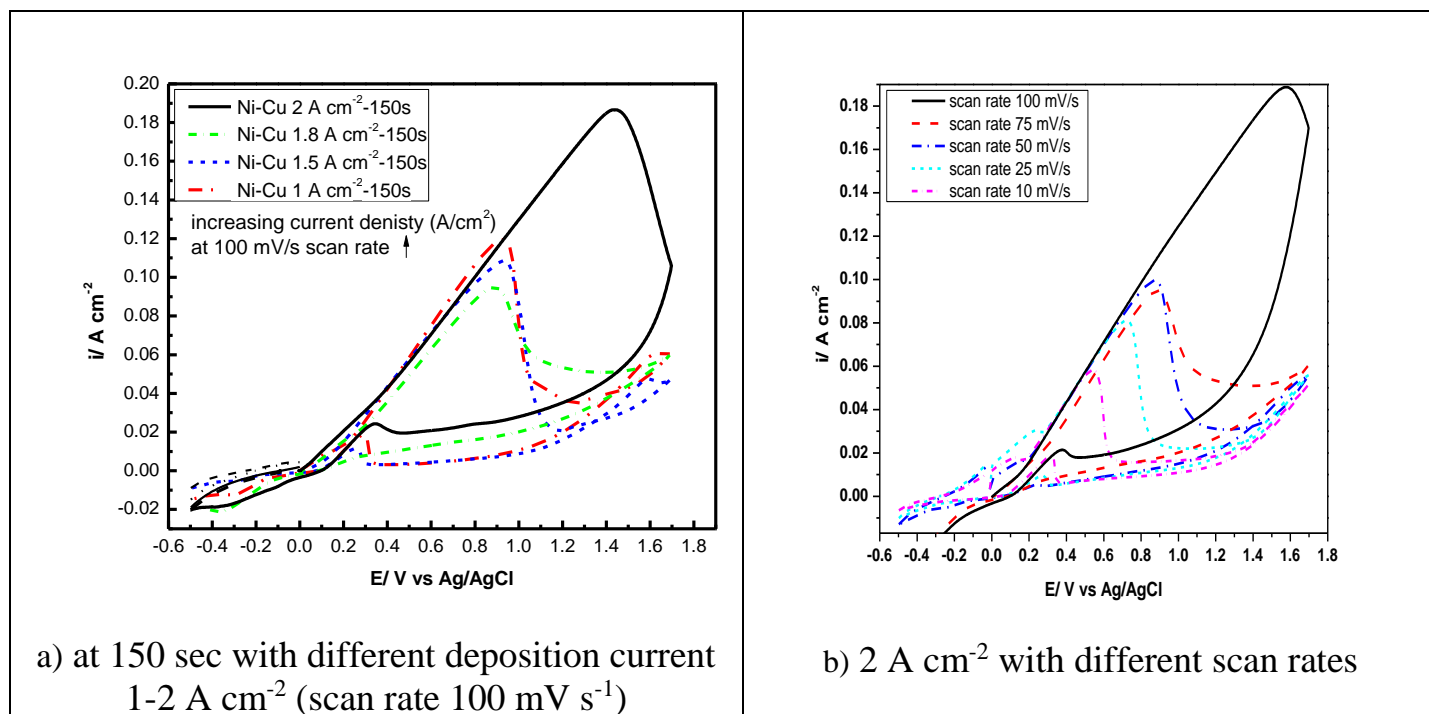
Figure 7. Cyclic voltammograms of porous Ni-Cu electrodeposited alloys tested in 1M methanol acidic solution, the comparison between different parameters.

In the forward direction, the observed peak is due to the oxidation of freshly chemisorbed species coming from methanol adsorption (equation 1). Meanwhile, in the backward direction, the oxidation corresponds to the removal of the carbonaceous species (CO gas) those have not completely oxidized in the forward scan. The oxidation of intermediate, mainly CO, as shown in equation (4) [36].

$$Ni - CO_{ads} + CO - OH_{ads}\ \rightarrow\ CO_2 + H^+ + e^- \quad\quad\quad (4)$$

The effect of the potential scan rate on the voltammetric response of porous Ni–Cu layers deposited at current density 2 A cm^{-2} for 150 s is presented in Fig.7-b. The highest peak intensity was registered upon applying a scanning rate of 100 mv/sec.

It is also observed from figure 6 that as the deposition time increases, there is a decrease of forward and backword peaks separation. High peak separation in the cyclic voltammograms of porous Ni-Cu materials has been attributed to both ohmic resistance due to the electrolyte diffusion through the pores and polarization of the electrode material [29].

Menshykau and Compton [37] have reported that the deposit porosity and morphology can significantly affect the shape of voltammograms, particularly, peak current and separation. This is due to occurrence of a thin layer diffusion regime.

In conclusion, increasing both the applied current density and the deposition time will lead to an increase of the forward peak intensity and total charge measured by cyclic voltammetry leading to an improvement of the electrochemical activity of the Ni-Cu porous films (Fig. 7-a).

3.5 Electrochemical Impedance-EIS Test

a) 1 A cm^{-2} b) 1.5 A cm^{-2}

c) 1.8 A cm^{-2}

d) 2 A cm^{-2}.
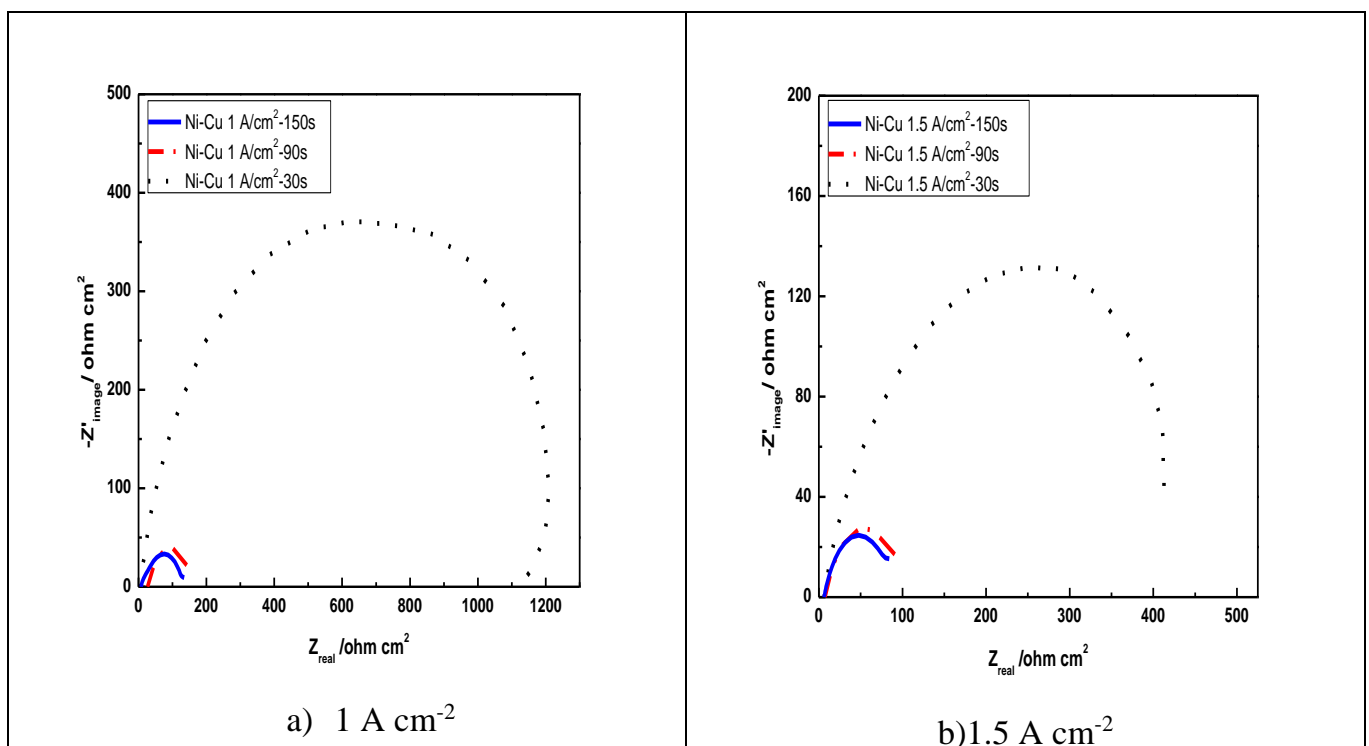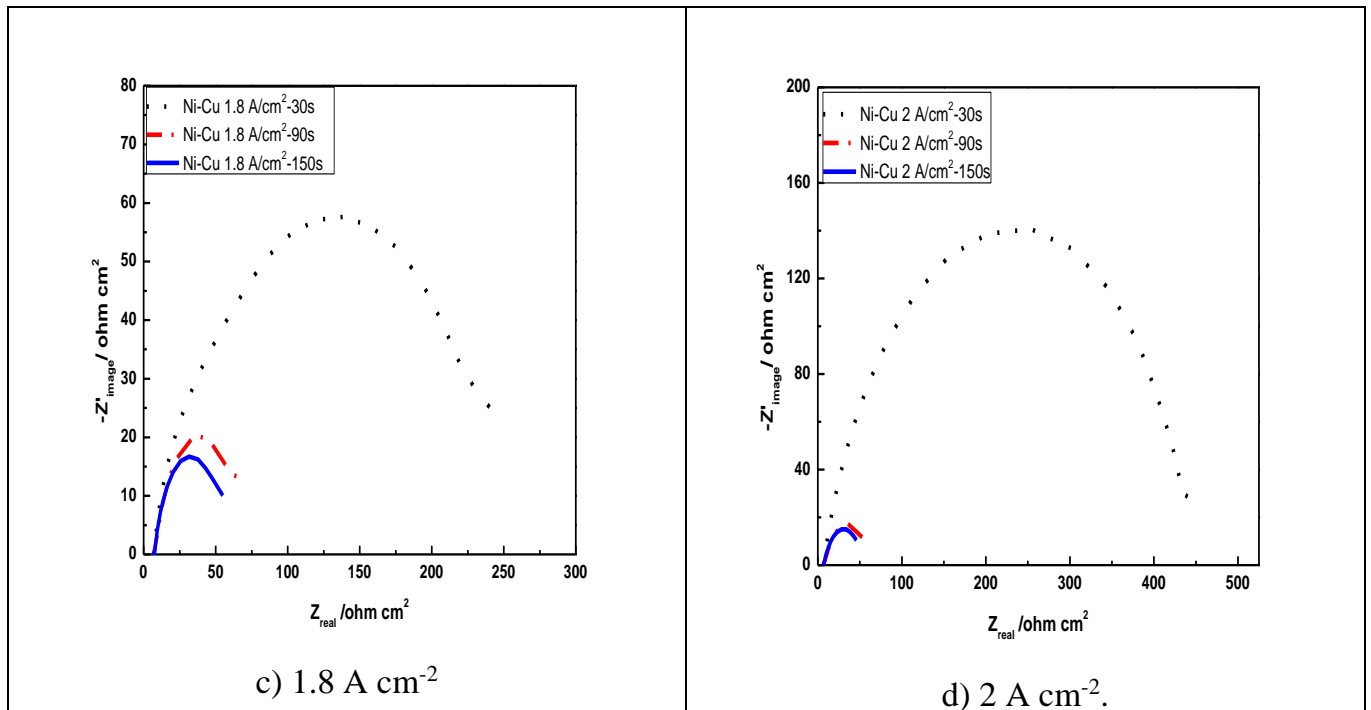
Figure 8. EIS Nyquist plots porous Ni-Cu electrodeposited alloys tested in acidic 1M methanol acidic solution as a function of current density as well as electrodeposition time at 25 °C.

Figure 8 shows EIS Nyquist representation data for porous Ni-Cu layers electrodeposited at different deposition time and current density, using 1M C_2H_5OH acidic solution at 25 ^{0}C. The Nyquist plot for each electrodeposition condition is composed of two semi-circles.

From figures 8-a-d, it can be concluded that layers electrodeposited at longer time, showed a smaller arc diameter meaning that they have the lowest impedance to charge transfer. The lowest arc diameter was registered for porous Ni-Cu layers electrodeposited at 2 Amp/cm^2 for 150 sec.

Table 5. Electrochemical impedance EIS parameters of porous Ni-Cu electrodeposited alloys at different deposition current densities and different times in acidic 1M Methanol solution at 25 °C.

Electrode	R$_p$ (ohm)	R$_s$ (ohm)	Y^0 (S*s^a)	alpha
Ni-Cu 1A/cm^2-30 s	1301.0	6.1	0.00009	0.7672
Ni-Cu 1A/cm^2-90 s	139.1	6.6	0.00556	0.6373
Ni-Cu 1A/cm^2-150 s	132.2	7.4	0.00322	0.5678
Ni-Cu 1.5A/cm^2-30 s	439.9	6.0	0.00129	0.6854
Ni-Cu 1.5A/cm^2-90 s	95.0	7.1	0.00798	0.6609
Ni-Cu 1.5A/cm^2-150 s	83.7	6.2	0.00651	0.6789
Ni-Cu 1.8A/cm^2-30 s	236.9	6.6	0.00234	0.6192
Ni-Cu 1.8A/cm^2-90 s	71.1	6.8	0.01783	0.6435

Ni-Cu 1.8A/cm^2-150 s	53.5	7.2	0.02961	0.7147
Ni-Cu 2A/cm^2-30 s	442.6	6.9	0.00046	0.7454
Ni-Cu 2A/cm^2-90 s	59.6	6.8	0.00939	0.6518
Ni-Cu 2A/cm^2-150 s	51.7	6.6	0.01865	0.662

Table 5 summarizes the data by fitting EIS experimental recorded at various deposition current density and time which tested in 1 M methanol acidic solution of the investigated electrocatalytic coatings. The solution resistance (R_s) changed in all the specimens by small degree due to using the same electrolyte.

In addition, it can be observed that the polarization resistance or charge transfer resistance (R_p) decreased as the applied current density as well as electrodeposition time increased.
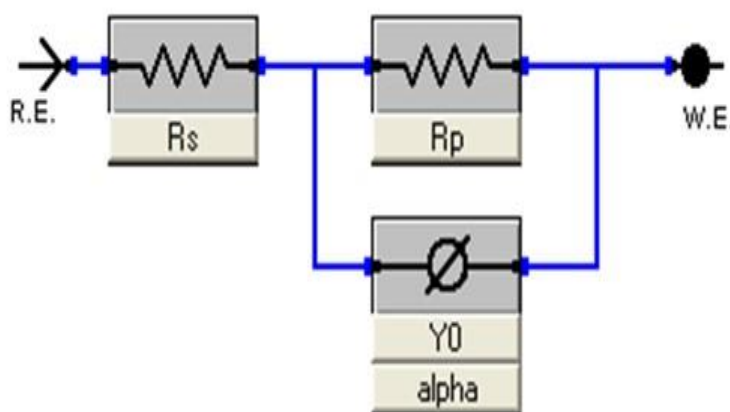
Figure 9. Equivalent circuit represents the behavior of porous Ni-Cu electrodeposited layers tested in 1M methanol acidic solution at 25 °C, *where R_s, the solution resistance, R_p polarization resistance Ø, Constant Phase Element (CPE)*

Figure 9 represents the equivalent circuit model of the electrochemical interface used to explain electrocatalytic activity of deposited electrode, where R_s is the solution resistance, R_p polarization resistance and Ø is constant phase element (CPE). There is an excellent agreement between the experimental and fitting data.

Table 6 compare our results of electrochemical tests results of Ni-C NPMFs with reports in the literature on anode catalysts for direct methanol fuel cell. According to this work, the lowest polarization resistance (51.7 ohms), was detected for porous Ni-Cu layers electrodeposited at 2 Amp/cm^2 for 150 sec. In this case, the deposited layer contains 87.86% Ni and 10.80% Cu and 1.34% O. This polarization value can be considered as a promising value compared with Pt-based nanodeposites. According to Jafarian [38], copper does not undergo redox processes in the potential range of nickel's electro-activity and the modification of nickel by copper has proved to enhance its electro-catalytic performance in methanol electro-oxidation.

Table 6. Matrix for comparing our electrochemical tests results of Ni-Cu NPMFs with reports in the literature on anode catalysts for direct methanol fuel cell.

Catalyst	β_a mV/decade	β_c mV/decade	I_{corr} (µA/cm²)	Rp (Ω)
Ni-Cu (20%Cu) – Current Work	149	653	824	51.7
Ni-Co (16% Co) [32]	10.4	29.2	2.37	1007.1
Ni-Co (33.5%Co) [33]	249	275	1027	55.7
Ni [38]	-	-	-	875.8
Pt–Ru/Al$_2$O$_3$–C (1:1) [40]	-		-	22.1

4. CONCLUSION

Porous Ni–Cu NPMFs, with porous 3 D dendritic structure, have been deposited on stainless steel substrates by controlling the applied current densities above 1 A cm^{-2}. The morphology of the deposited films was affected by the current density and deposition time. At low current density and short deposition time (30 sec), smooth films composed of angular grains, with few randomly distributed isolated dendrites were detected. At high current density, typical ramified dendritic morphology was developed. According to EDX analysis, increasing both the deposition time and applied current density leads to an increase of the Ni content in the deposited alloys. From potentiodynamic test results, increasing the deposition current density as well as deposition time lead to more anodic and current density, reflecting high electrocatalytic behavior towards methanol oxidation. Higher forward peak intensity and total charge measured by cyclic voltammetry increased under the effect of higher applied current density and longer deposition time having a positive effect on the electrochemical activity of the Ni-Cu NPMFs deposited. From the EIS test, it can be observed that the charge transfer resistance (R_P) decreased as the current density as well as electrodeposition time increased. The lowest polarization resistance was detected for porous Ni-Cu layers electrodeposited at 2 Amp/cm^2 for 150 sec (51 ohms). In this case, the deposited layer is composed of 70.66% Ni, 19.98%Cu and 1.36% O.

References

1. S. Arisetty, A. K. Prasad and S.G. Advani, *J. Power Sources*, 165 (2007) 49.
2. P. Joghee, J. N. Malik, S. Pylypenko and R. O'Hayre, *MRS Ener. Sustain. A Review*, 2 (2015) 1.
3. L. S. Grigorii, Beilstein *J. Nanotech.*, 5 (2014) 1399.
4. S. R. Narayanan, A. Kindler, B. Jeffries-Nakamura, W. Chun, H. Frank, M. Smith, T.I. Valdez, S. Surampudi, and G. Halpert, Proceed.of 11th Annual Batt. Conf. on Appl. and Adv., 1996, 113.
5. M. A. Smith, A. L. Ocampo, M. A. Espinosa-Medina and P. J. Sebastian, *J. Power Sources*, 124 (2003) 59.
6. S. M. J. Zaidi, S. D. Mikhailenko, G. P. Robertson, M. D. Guiver and S. Kaliaguine, *J. Membrane Sci.*, 173 (2000) 17.

7. N. K. Beck, B. Steiger, G. G. Scherer and A. Wokaun, *Fuel Cells*, 1 (2006) 26.
8. P. Piela, R. Fields and P. Zelenay, *J. Electrochem. Soc*., 153 (2006) A1902.
9. D. M. F. Santos, S. Eugenio, C.A.C. Sequeira and M. F. Montemor, *ECS Trans.,* 64 (2015) 9.
10. S. Euge´nio, T. M. Silva, M. J. Carmezim, R. G. Duarte and M. F. Montemor, *J. Appl. Electrochem.,* 44(2014) 455.
11. C. Woo-Sung, J. Hye-Ran, K. Se-Hun, L. Jong-Won, L. Meilin and S. Heon-Cheol, *J. Mater. Chem.,* 22 (2012) 1028.
12. Abdel-Karim, R.; El-Raghy. S. M., Advanced Materials and their Applications - Micro to Nano Scale, One Central Press, (2017) London, UK, 69-91.
13. R. Ramkumarb, S. Dheenadayalana and R. Pattabiraman, *J. Power Sources*, 69 (1997) 75.
14. M. C. Gutiérrez, M. J. Hortigüela, J. M. Amarilla, R. Jiménez, M. L. Ferrer and F. DelMonte, *J. Phys. Chem.* C, 111 (2007) 5557.
15. Y. Yu, Y. Cheng, M. Guo, C. Li and J. Hu, *RSC Adv*., 7 (2017) 39539.
16. J. Yang, J. Tan, F. Yang, X. Li, X. Liu and D. Ma, Electrochem. *Commun.* , 23 (2012)13.
17. B. J. Plowman, L. A. Jones and S. K. Bhargava, *Chem. Commun*., 51 (2015) 4331.
18. Z. Li, M. Ruan, L. Du, G. Wen, C. Dong and H. W. Li, *J. Electroanalyt. Chem*., 805 (2017) 47.
19. P. Arunachalam, M. A. Ghanem, A. M Al-Mayouf and M. Al-shalwi, *Mat. Lett.* , 196 (2017) 365.
20. L. Wang, G. Zhang, Y. Liu, W. Li, W. Lu and H. Huang, *Nanoscale*, 8 (2016) 11256.
21. L. S. Yuan, Y. X. Zheng, M. L. Jia, S. J. Zhang, X. L. Wang and C. Peng, *Electrochimica Acta*, 154 (2015) 54.
22. M. Y. Gao, C. Yang, Q. B. Zhang, Y.W. Yu, Y. X. Hua, Y. Li and P. Dong, *Electrochimica Acta*, 215 (2016) 609.
23. F. Wolfart, B. R. Brito, L. F. Marchesi, M. Vidotti and J. Braz, *Chem. Soc.,* 28 (2017) 1586. 24.
24. D. S. P. Cardoso, S. Eugénio, T. M. Silva, D. M. F. Santos, C. A. C. Sequeira and M. F. Montemor, *RSC adv*., 5 (2015) 43456.
25. E. Pellicer, S. Pané , V. Panagiotopoulou, S. Fusco, K. M. Sivaraman, S. Suriñach , M. D. Baró, B. J. Nelson and J. Sort, *Int. J. Electrochem. Sci*., 7 (2012) 4014.
26. L. Wei, K. Goh, Ö. Birer, H. E. Karahan, J. Chang, S. Zhai, X. Chen and Y. Chen, *Nanoscale*, 9 (2017) 4401.
27. J. Zhang, M. D. Baro, E. Pellicer and J. Sort, *Nanoscale*, 6 (2014) 12490.
28. W. Zhang, C. Ding, A. Wang and Y. Zeng, *J. Electrochem. Soc*., 162 (2015) D365.
29. S. Euge´nio, T. M. Silva, M. J. Carmezim, R. G. Duarte and M. F. Montemor, *J. Appl. Electrochem.,* 44(2014) 455.
30. D. M. F. Santos, S. Eugenio, C. A. C. Sequeira and M. F. Montemor, *ECS Trans*., 64 (2015) 9.
31. N. D. Nikolic, K. I. Popov, L. J. Pavlovic and M. G. Pavlovic, *J. Solid State Electrochem*., 11(2007) 667.
32. R. Abdel-Karim, M. Ramadan, H. A. Ahmed, and S. M. El-Raghy, *J. Nanomat., Article* ID 9870732 (2018) 13 pages.
33. S. Paul and S. k. Naimuddin, *J. Fuel Cell Sci. Technol*., 43 (2015) 1004.
34. S. Wasmus and A. Kuver, *J. Electroanalyt. Chemistry*, 461(1999) 14.
35. S. Mohan and S. O. Bade Shrestha, *Open Fuels & Ener. Sci. J*., 2 (2009) 124.
36. S. S. Gupta, S. Singh and J. Datta, *Mater. Chem. Phys.,* 116 (2009) 223.
37. D. Menshykau and R. G. Compton, *Electroanalysis,* 20 (2008) 2387.
38. M. Jafarian, R.B. Moghaddam, M.G. Mahjani and F. Gobal, *J Appl Electroche*, 36 (2006), 913.
39. H. Beydaghi1, M. Javanbakht, A. Bagheri, H. Ghafarian-Zahmatkesh, Khadijeh Hooshyari, *IJHFC,* 1(2017) 1.

40. S. Das and P. P. Kundu, *RSC Adv*., 5 (2015), 93539.